

## Quantification of renal diffusion-weighted images using a bi-exponential model

J. L. Zhang<sup>1</sup>, E. E. Sigmund<sup>1</sup>, H. Rusinek<sup>1</sup>, H. Chandarana<sup>1</sup>, Q. Chen<sup>1</sup>, P. Storey<sup>1</sup>, L. Bokacheva<sup>1</sup>, and V. S. Lee<sup>1</sup>

<sup>1</sup>Radiology, New York University, New York, NY, United States

### Introduction

Although well-studied in applications in the brain (1), the perfusion contribution to diffusion signal decay has not been quantified in renal applications. This effect, sometimes called “intravoxel incoherent motion (IVIM)” contributes substantially to overall signal decay in kidney, and it has been attributed to renal capillary perfusion (2). Since in kidney a large fraction (~20%) of water is filtered into tubules, we hypothesize that tubular fluid flow also contributes to IVIM. If confirmed, quantification of IVIM could lead to non-invasive assessment of renal vascular and tubular functions. In this study, we acquired volunteer DWI data with multiple diffusion weightings and multiple repetitions, and used a bi-exponential model for data analysis, with the aim of accurately quantifying the diffusion and IVIM effect in various tissues of kidney.

### Methods

Two healthy volunteers (39 and 43 years) were scanned on a 3T MRI (Tim Trio, Siemens) with a spine coil and body array coil combination. Coronal single-shot echo planar DWI sequence were acquired using: 5 slices; slice thickness 6 mm; FOV 345×410 mm; matrix 162×192; TR/TE 2000/78 ms, 3-Scan Trace mode, parallel imaging (iPat) = 2. Diffusion imaging using 27 b values from 0 to 1300 s/mm<sup>2</sup> with a 50s/mm<sup>2</sup> step was performed with nine (Case 1) and two (Case 2) repetitions. Each repetition took about 2.5 minutes. The volunteers were asked to breathe shallowly. Images were co-registered using cross correlation method to correct for respiratory motion. Registered repetitions were then averaged prior to analysis.

On the unweighted images ( $S_0$ ) the kidney was partitioned into renal cortex and medulla. On one kidney an incidental cyst was also analyzed as a separate region. For each tissue regional signals were fitted by

$$S = S_0 \cdot [(1 - F_p) \cdot \exp(-b \cdot \text{ADC}_D) + F_p \cdot \exp(-b \cdot \text{ADC}_P)] \quad [1]$$

where  $\text{ADC}_D$  represents pure diffusion coefficient,  $F_p$  volume fraction of high flow voxels (vessels, tubules), and  $\text{ADC}_P$  denotes the pseudo-diffusion coefficient due to perfusion (2). We also considered a derived parameter,  $P_p = F_p \times \text{ADC}_P$ , which is physically analogous to renal plasma flow (RPF) as derived from contrast-enhanced perfusion imaging (1). Fitting of Eq [1] was performed over the range ( $0 \leq b \leq 800$  s/mm<sup>2</sup>) to ensure sufficiently high SNR. Root means square residue (RMS) expressed as a percentage of  $S_0$  was calculated for each fit.

To generate parameter maps, monoexponential fitting was first performed, and for the voxels with residual error larger than noise level, Eq [1] was fitted, producing maps for  $S_0$ ,  $\text{ADC}_D$ ,  $F_p$ ,  $\text{ADC}_P$  and  $P_p$ .

### Results / Discussion

Table 1: Parameter values by mono- and bi-exponential fittings in ROI analysis

		Mono-exp		Bi-exponential			RMS
		$\text{ADC}_{\text{tot}}$ ( $\times 10^{-3}$ mm <sup>2</sup> /s)	$\text{ADC}_D$ ( $\times 10^{-3}$ mm <sup>2</sup> /s)	$F_p$	$\text{ADC}_P$ ( $\times 10^{-3}$ mm <sup>2</sup> /s)	$P_p$ ( $\times 10^{-3}$ mm <sup>2</sup> /s)	
Cortex	Case1	2.2±0.1	1.5±0.1	0.38±0.02	11.8±1.0	4.5±0.2	0.7%
	Case2	2.2±0.1	1.5±0.1	0.33±0.04	13.8±2.5	4.5±0.5	1.4%
Medulla	Case1	2.1±0.1	1.5±0.1	0.32±0.02	17.3±1.7	5.5±0.4	0.9%
	Case2	2.0±0.1	1.4±0.1	0.31±0.04	9.8±1.8	3.0±0.3	1.1%
Cyst	Case1	2.3±0.1	1.9±0.1	0.21±0.03	9.1±1.5	2.0±0.1	0.6%

Figure 1 shows the fitting curves for the tissue signals of Case 1 using Eq. [1]. Across the kidney,  $\text{ADC}_D$  and  $F_p$  showed similar patterns (Table 1, Fig.2).  $\text{ADC}_D$  was comparable for cortex and medulla, while significantly higher in the cyst.  $\text{ADC}_D$  difference between renal parenchyma and cyst ( $0.4 \times 10^{-3}$  mm<sup>2</sup>/s) was more than two-fold larger than for  $\text{ADC}_{\text{tot}}$  ( $\sim 0.15 \times 10^{-3}$  mm<sup>2</sup>/s).  $F_p$  in cortex was higher than in medulla, and  $F_p$  in cyst was the lowest.  $\text{ADC}_P$  showed consistent values in the two cases in the cortex but more variable in the medulla. Similar behavior is seen in the perfusion product  $P_p$ .

Compared to  $\text{ADC}_D$ , the perfusion-related parameters  $F_p$  and  $\text{ADC}_P$  suffered from lower precision for voxel-wise analysis (Fig. 2). This is partially ameliorated by forming the perfusion product  $P_p$ , whose map shows a smoother texture.

Lack of contrast for  $\text{ADC}_D$  between cortex and medulla suggests that the commonly observed  $\text{ADC}_{\text{tot}}$  contrast between cortex and medulla is in fact due to IVIM effect.  $F_p$ , which corresponds to volume fraction of voxels exhibiting high water flow, was estimated as 32%~38% for cortex and 31%~32% for medulla. These values are much higher than 5%~15% observed with other perfusion-based measurements. Hence, tubular flow and water reabsorption may contribute substantially to the IVIM effect. It follows that the variability in  $\text{ADC}_P$  may be due to the differences in tubular factors such as hydration status.

### Conclusions

Quantitative assessment of renal diffusion and IVIM effects in diffusion-weighted imaging was achieved using a free-breathing multi-repetition sequence and bi-exponential analysis.  $\text{ADC}_{\text{tot}}$  contrast between cortex and medulla is predominantly due to the IVIM effect, and the IVIM effect (so-called “perfusion”) likely contains a significant tubular contribution. Further work is needed to separate perfusion and tubular components.

### References

1. Lebihan et al. Magn Reson Med 27:171-178 (1992). 2. Thoeny et al. Radiology 235:911-917 (2005).

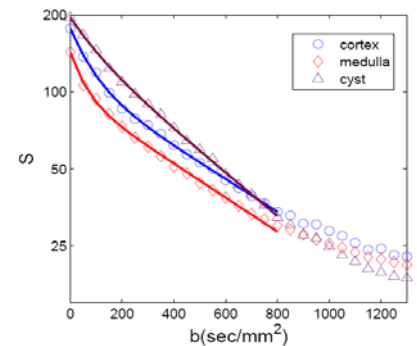


Figure 1: Diffusion-weighted renal tissue signals.

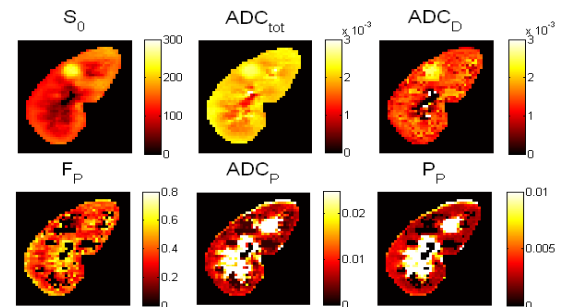


Figure 2: Parameter maps of mono- and biexponential analysis.